Order-of-Magnitude Scaling of the Cathode Region in an Axisymmetric Transferred Electric Arc

P.F. MENDEZ, M.A. RAMIREZ, G. TRAPAGA, and T.W. EAGAR

A new technique of order-of-magnitude scaling (OMS) has been applied to the mathematical modeling of the cathode region of a long gas tungsten arc (GTA). The estimations obtained are combined with numerical calculations; thus, important features of both techniques are considered simultaneously: the high precision of numerical modeling and the generality and simplicity of algebraic expressions. Power-law expressions for the estimations of characteristic unknowns such as maximum pressure in the cathode spot and maximum plasma velocity are obtained and are consistent with previous analytical or asymptotic work. Dimensional analysis is used to identify dimensionless groups governing the system, and asymptotic considerations are used to identify two dimensionless groups (the Reynolds number and the dimensionless arc length) as the most significant ones governing momentum transfer in the cathode region. The estimations obtained are calibrated with functions that depend only on these two most significant dimensionless groups. It is suggested that the numerical results for different cases can be reduced to a single general map.

I. INTRODUCTION

THE main goal of this work is to demonstrate a new technique of order-of-magnitude scaling (OMS)[1] to a complex engineering problem: the welding arc. This technique allows the simultaneous use of dimensional analysis and asymptotic considerations such as dominant balance.[2] The main difference between OMS and previous work in the field of dimensional analysis and asymptotic considerations[3,4,5] is that in OMS, the unknown functions are required to vary smoothly between the edges of the domain. This way, these functions and their derivatives up to a second order have special properties and can be characterized by a single characteristic value. Dimensional analysis provides an exact description of the functional dependence in the problem, based on a complete set of dimensionless groups. The asymptotic considerations determine the functional expression of the dimensionless groups and describe their relative importance. This way, dimensionless groups of little influence can be discarded without significant loss in accuracy. The asymptotic considerations also provide scaling for the problem. The scaling factors and relevant dimensionless groups obtained can be combined with numerical calculations in order to express these results in a general, dimensionless form. The OMS technique is a useful tool for a wide variety of problems, with many driving forces described by a set of differential equations. For the sake of simplicity using this new tool, the present analysis focuses on the fluid motion of the plasma in the cathode region of the arc, where the electromagnetic forces are dominant.[6] Due to its small size relative to the rest of the arc, the cathode region can be assumed to be isothermal, in contrast to other regions in the domain, where significant temperature gradients are present. Other regions of the arc cannot be assumed to be isothermal. In these cases, the OMS technique would still be useful, but new equations (*e.g.*, conservation of energy) must be considered. In such cases, the complexity of the problem would increase substantially, with many more parameters necessary to describe the problem and many more balances and asymptotic regimes to analyze.

Previous attempts have been made to provide general and simple expressions that capture the behavior of the arc. Some of these have been derived using dimensional analysis or asymptotic analysis.[6±14] In addition, some contributions to the behavior of the arc involved analysis of results obtained from mathematical models.[6,15±19] The results obtained herein are consistent with the existing literature, but this work goes further by determining that the discrepancy between the simple algebraic expressions and exact solutions can be almost completely captured by the Reynolds number and the dimensionless arc length. The thermal properties of the plasma have only a secondary effect through the temperature-dependent physical properties of the plasma for the range between 200 and 2000 A, at least in argon and air systems.

II. DESCRIPTION OF THE PROBLEM

The focus of this article is on the cathode region of a long arc. This region (represented in Figure 1) is defined as that contained within an area of R_C in the radial direction and extending for a length of Z_S beyond the cathode boundary layer in the axial direction. A long arc is such that the position of the anode has little effect on the behavior of the cathode region. A convenient way to define the characteristic length Z_S is*

*For an explanation of the notation, refer to Fig. 1 and the last paragraph of this article.

P.F. MENDEZ, Postdoctoral Associate, and T.W. EAGAR, Professor of Materials Engineering, are with the Department of Materials Science and Engineering, Massachusetts Institute of Technology, Cambridge, MA 02139. M.A. RAMIREZ, formerly Graduate Student, Department of Materials Science and Engineering, Massachusetts Institute of Technology, is Professor, Instituto Tecnologico de Morelia, 58120 Morelia, Mich., Mexico. G. TRAPAGA, formerly Principal Research Associate, Department of Materials Science and Engineering, Massachusetts Institute of Technology, is Professor, Laboratorio de Investigacion en Materiales, CINVESTAV-IPN, 76230 Queretaro, Qro., Mexico.

Manuscript submitted May 18, 2000.

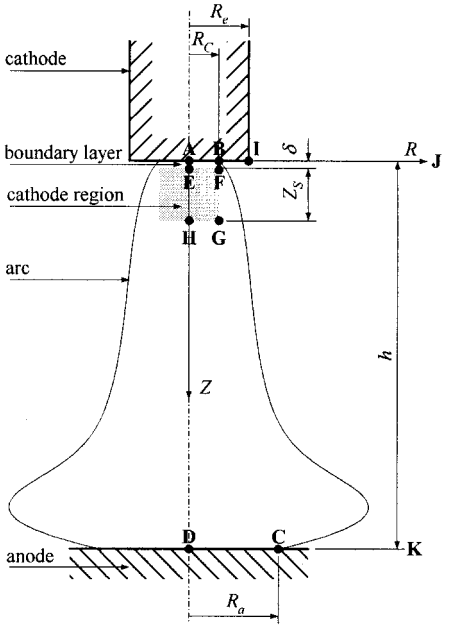

Fig. 1–Long GTA welding arc and its cathode region. In a long arc, the arc length (h) is significantly longer than the characteristic distance Z_S.

$$Z_S = V_{ZS}/\max(\partial V_Z/\partial Z) \qquad [1]$$

The cathode spot radius can be calculated as $R_C = (I/\pi J_C)^{1/2}$, where the critical current density (J_C) depends only on the electrode temperature (for the numerical simulations, it was assumed that $J_C = 6.5 \times 10^7$ A/m^2[20] for a tungsten electrode and that $J_C = 4.4 \times 10^7$ A/m^2[21] for a graphite electrode).

Experiments[15] and numerical simulations, including those to be discussed subsequently, indicate that the temperature variations within the cathode region are small compared to the maximum temperature jump in the arc. This region will be assumed to be isothermal, with the physical properties corresponding to the maximum temperature in the arc ($T_{\max}$). The governing equations can, therefore, be simplified as follows:

$$\frac{1}{R}\frac{\partial}{\partial R}(RV_R) + \frac{\partial V_Z}{\partial Z} = 0 \qquad [2]$$

$$\rho\left(V_R\frac{\partial V_R}{\partial R} + V_Z\frac{\partial V_R}{\partial Z}\right) = -\frac{\partial P}{\partial R} + \mu\left(\frac{\partial}{\partial R}\left(\frac{1}{R}\frac{\partial}{\partial R}(RV_R)\right) + \frac{\partial^2 V_R}{\partial Z^2}\right) - J_Z B \qquad [3]$$

$$\rho\left(V_R\frac{\partial V_Z}{\partial R} + V_Z\frac{\partial V_Z}{\partial Z}\right) = -\frac{\partial P}{\partial Z} + \mu\left(\frac{1}{R}\frac{\partial}{\partial R}\left(R\frac{\partial V_Z}{\partial R}\right) + \frac{\partial^2 V_Z}{\partial Z^2}\right) + J_R B \qquad [4]$$

$$\mu_0 J_R = -\frac{\partial B}{\partial Z} \qquad [5]$$

$$\mu_0 J_Z = \frac{1}{R}\frac{\partial}{\partial R}(RB) \qquad [6]$$

Table I. Boundary Conditions for the Scaling of the Electromagnetic Field

	A	B	C	D
B	0	$\frac{1}{2}\mu_0 J_C R_C$	$\frac{1}{2}\mu_0 J_C R_C^2/R_a$	0

Table II. Boundary Conditions for Scaling of the Fluid Flow

	E	F	G	H
V_R	0	$\approx -V_{RS}$	≈ 0	0
V_Z	≈ 0	≈ 0	≈ 0	$\approx V_{ZS}$

$$\frac{\partial^2 B}{\partial Z^2} + \frac{\partial}{\partial R}\left(\frac{1}{R}\frac{\partial}{\partial R}(RB)\right) = 0 \qquad [7]$$

In the previous set of equations, Eq. [2] is the equation of conservation of mass; Eqs. [3] and [4] are the equations of conservation of momentum in the R and Z components, respectively; Eqs. [5] and [6] represent Ampere's law in R and Z, respectively; and Eq. [7] is the equation of conservation of the magnetic field. In these equations, the following assumptions are made: an isothermal plasma (therefore, constant density and viscosity values corresponding to the maximum temperature in the cathode region); an axisymmetric, laminar flow; a steady state (this implies a d.c. arc, or slow current variations); and no magnetic convection, because the magnetic Reynolds number is very small. The magnetic Reynolds number is a measure of the ratio between the induced magnetic field (due to the conductive fluid motion) and the imposed magnetic field;[22] its expression in this problem is $\mathrm{Re}_m = V_{ZS} Z_S \sigma_e \mu_0$ and it varies between 10^{-3} and 10^{-1} for the cases studied here. The boundary conditions for the scaling of the system are listed in Tables I and II.

III. SCALING OF THE ELECTROMAGNETIC FIELD

In order to use dimensional analysis in a problem, it is necessary to define two sets: the complete set of parameters, $\{P\}$, and its subset of dimensionally independent parameters, $\{P_k\}$. The set $\{P\}$ contains all of the parameters necessary to completely describe the problem. All of the elements of $\{P\}$ are independent, which means that no element can be obtained as a function of the remaining elements. The set $\{P_k\}$ contains a subset of k elements of $\{P\}$, such that the units in each element are independent. Set $\{\Pi\}$ contains the independent dimensionless groups generated by the application of dimensional analysis. Its number of elements is m, and it is calculated using Buckingham's theorem:[23] $m = n - k$, where n is the number of elements of $\{P\}$.

Because constant properties are used, the governing equations for the electromagnetic field can be decoupled. The equations for the electromagnetic field contain a complete set of parameters, $\{P\} = \{\mu_0, R_c, J_c, R_a, h\}$, with the following subset of dimensionally independent parameters: $\{P_k\} = \{\mu_0, R_c, J_c\}$. Therefore, only two dimensionless groups are necessary to describe this system: $\{\Pi\} = \{h/R_C, R_a/R_C\}$. The boundary conditions for the scaling of the

electromagnetic field are represented in Table I. Previous knowledge of the problem (from experiments and numerical models) indicates that the functions vary smoothly within the corner points outlining the cathode region; this is an important requirement for the application of OMS.

The functions describing the electromagnetic field can be scaled with the following relationships:

$$R = R_a r' \quad [8]$$

$$Z = hz' \quad [9]$$

$$J_R(R,Z) = J_{RS} j_r(r',z') \quad [10]$$

$$J_Z(R,Z) = J_C j_z(r',z') \quad [11]$$

$$B(R,Z) = B_s r' \left(1 + \left(\frac{R_a^2}{R_c^2} - 1\right) b(r',z')\right) \quad [12]$$

where

$$B_S = \frac{1}{2}\mu_0 \frac{R_C^2}{R_a} J_C$$

The scaling factors R_a, h, J_{RS}, J_C, and B_S are characteristic values, of which R_a and J_{RS} are unknown. The scaling of $B(R, Z)$ is such that $b(r', z') = 1$ at point B in Figure 1, $b(r', z') = 0$ at point C in Figure 1, and $B(R, Z)$ increases linearly at $R = 0$, as Eqs. [5] through [7] indicate. The radius of the anode spot (R_a) depends on the electrical properties of the plasma, which are determined by heat transfer in the arc. The characteristic value J_{RS} could be estimated by balancing Eq. [5]. Normally, for welding arcs, $\Delta R/R_C > 1$, where $\Delta R = R_a - R_C$. The previous scaling relationships are valid for flat- or almost-flat-tip electrodes. The dominant component of the radial current density in sharper electrodes is given directly by the critical current density generated by thermionic emission.

When these scaling relationships are replaced into the governing equations for the electromagnetic field (Eqs. [5] through [7]), the estimation of the characteristic radial current density J_{RS} can be obtained from Eq. [5] using the dominant-balance technique.

$$\hat{J}_{RS} = \begin{cases} J_C \dfrac{R_c \Delta R}{h R_a} & \text{for } \dfrac{\Delta R}{R_C} < 1 \\ J_C \dfrac{\Delta R^2}{h R_a} & \text{for } \dfrac{\Delta R}{R_C} \geq 1 \end{cases} \quad [13]$$

IV. SCALING OF FLUID FLOW

The equations governing the coupled electromagnetic field and fluid flow in the cathode region (Eqs. [2] through [7]) contain a complete set of parameters, $\{P\} = \{\rho, \mu, \mu_0, R_c, J_c, R_a, h, R_e\}$, with the following subset of dimensionally independent parameters: $\{P_k\} = \{\mu_0, R_c, J_c, \rho\}$. The complete set of dimensionless groups related to the fluid flow is $\{\Pi\} = \{\mathrm{Re}, h/R_C, R_a/R_C, R_e/R_C\}$, where $\mathrm{Re} = \rho \hat{V}_{ZS} \hat{V}_S / \mu$. Because R_a is the only element of {P} that depends on heat transfer in the arc, the dimensionless group R_a/R_C will be neglected in this isothermal formulation. The group R_e/R_C is also of little importance, because its influence is confined mainly to the cathode boundary layer, outside the cathode region. The boundary conditions for the scaling of the fluid flow are represented in Table II. Current knowledge about the problem (from experiments and numerical models) indicates that the functions vary smoothly within the corner points.

The functions describing fluid flow can be scaled with the following relationships:

$$R = R_C r \quad [14]$$

$$Z = \delta + Z_S z \quad [15]$$

$$V_R(R,Z) = V_{RS} r v_r(r,z) \quad [16]$$

$$V_Z(R,Z) = V_{ZS}(v_{z0}(z) - f_{VZ2}(\mathrm{Re}, h/R_c) r^2 v_z(r,z)) \quad [17]$$

$$P(R,Z) = P_S p(r,z) \quad [18]$$

The scaling of $V_Z(R, Z)$ is such that it varies in a quadratic manner in R at $R = 0$, as Eqs. [2] through [4] indicate. These scaling relationships are replaced into the governing equations for the fluid flow (Eqs. [2] through [4]) for the application of the dominant-balance technique. This technique determines that the inertial forces are balanced by the plasma pressure and the electromagnetic forces in the equation of conservation of momentum in the radial direction, and that the plasma pressure balances the inertial forces in the equation of conservation of momentum in the axial direction. Viscous effects are secondary. With the dominant and balancing forces established, the characteristic values Z_S, V_{RS}, V_{ZS}, and P_S can be stimulated as

$$\hat{Z}_S = \frac{1}{2} R_C \quad [19]$$

$$\hat{V}_{RS} = \frac{1}{2} \frac{\mu_0^{1/2} \mathrm{R_C J_C}}{\rho^{1/2}} \quad [20]$$

$$\hat{V}_{ZS} = \frac{1}{2} \frac{\mu_0^{1/2} \mathrm{R_C J_C}}{\rho^{1/2}} \quad [21]$$

$$\hat{P}_S = \frac{1}{2} \mu_0 R_C^2 J_C^2 \quad [22]$$

The previous estimations are valid when all of the terms in the normalized governing equations (Eqs. [2] through [7]) have a magnitude of one or less. This is true for $\mathrm{Re} > 1$, $R_a/R_C > 2$, and $h/R_C > 1/2\ \Delta R^2/(R_a R_C)$. In order to further simplify the problem and avoid the effects of the anode on the cathode region, an additional condition is necessary: $h/Z_S \gg 1$. These conditions are met for all of the cases considered in the present analysis.

V. NUMERICAL ANALISIS

The formulation of the numerical model is also represented by the conservation Eqs. [2] through [7], described previously, plus an equation for the conservation of energy with the assumption of local thermodynamic equilibrium (LTE). Since the numerical model covers the whole domain and is not confined to only representing the cathode region, the boundary conditions include the cathode, the anode, and the column regions. The equation of conservation of energy includes the temperature dependence of thermophysical properties. The additional boundary conditions required to represent the system are summarized in Table III and include the following assumptions:

(1) nonslip conditions at the surface of the electrodes (zero velocity values);

Table III. Boundary Conditions for Numerical Representation of the Arc (The Domain Segments Make Reference to Figure 1)

	AB	BI	IJ	JK	DK	AD	BJ
V_Z	0	0	$\partial V_Z/\partial Z = 0$	$\partial V_Z/\partial R = 0$	0	$\partial V_Z/\partial R = 0$	–
V_R	0	0	0	$\partial V_Z/\partial Z = 0$	0	0	–
T	4000	$\partial T/\partial Z = 0$	1000	1000	2500	$\partial T/\partial R = 0$	–
B	$\mu_o Ir/2\pi R_c^2$	–	–	$\mu_o I/2\pi r$	$\partial B/\partial Z = 0$	B = 0	$\mu_o I/2\pi r$

(2) the temperatures at the electrodes are assumed to be constant at 2500 K on the anode and 4000 K on the cathode;[24]
(3) the boundary conditions must reflect the symmetry condition of no flow across the axis (line AD in Figure 1); and
(4) the magnetic flux density (B) at the cathode is obtained by assuming a constant value of J_C in the cathode spot of known radius, but a value of zero outside this spot.

The numerical solution of this problem is essentially the same as in Reference 20, where a more detailed discussion of the previous formulation and boundary conditions can be found. The process consisted of solving the electromagnetic components, which are coupled to the hydrodynamic equations, the latter having been solved using the commercial code Phoenics. A significant difference between the present work and that of Reference 20 is that a computing-power increase allowed the use of a mesh approximately 10 times denser.

Illustrative results of this model are shown in Figures 2 through 4. In a typical calculation, a grid of 60 × 60 nodes was employed, and each calculation normally took about 2 hours of CPU time on a PENTIUM* II-333 processor. Figure 2 shows the computed pressure (left-hand side) and velocity (right-hand side) fields for an argon arc produced under 200 A current, with an arc length of 10 mm. The figure shows the two characteristic high-pressure regions in the arc, namely, the one formed in the vicinity of the cathode, which counterbalances the electromagnetic forces (*i.e.*, the Maecker pressure), and the region close to the anode, caused by impingement of the jet. This pressure field is responsible for the velocity jet shown in the right-hand side of the figure. It is noted that the maximum velocity in this case is about 250 m/s.

*PENTIUM is a trademark of the Intel Corporation, Santa Clara, CA.

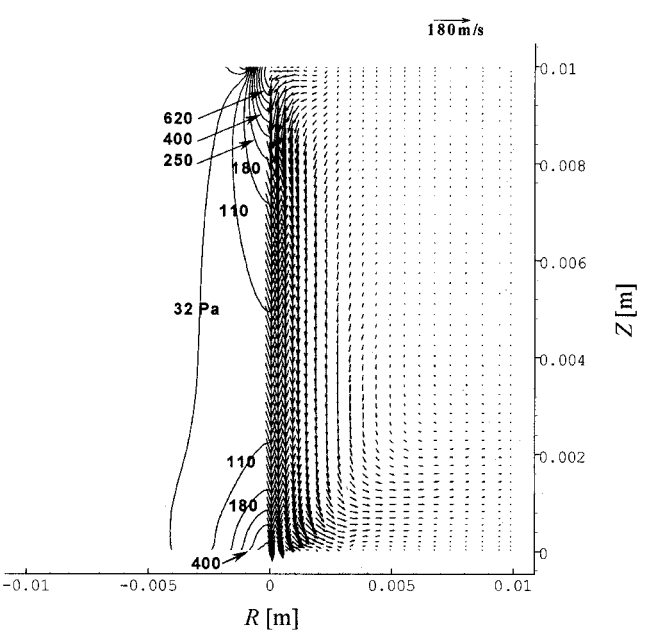

Fig. 2–Computed pressure (left) and velocity (right) fields for a 200 A, 10-mm-length argon arc. Pressure contours are relative to atmospheric pressure and are given in Pascal units.

The corresponding temperature results are shown in Figure 3, together with some experimental measurements carried out by Hsu *et al.*[15] As seen in the figure, the agreement between experiments and predictions is very good. The temperature range shown in the figure defines the conductive region of the arc and covers a wide range of values (*i.e.*, 11,000 to 21,600 K). It is interesting to note that the cathode region includes the maximum temperature and only covers a small range of temperatures (of about 500 K). This supports the hypothesis that the cathode region, as defined previously for OMS and superimposed in Figure 3, can be considered to be essentially isothermal.

Figure 4 shows predicted velocity and pressure profiles along the axis of symmetry for a 2160 A, 7 cm air arc. These conditions are the same used in velocity measurements by Bowman,[25] which are also included in the fure. As seen in the plot, reasonable agreement is observed between measured and predicted velocities. The shape of these profiles is consistent with the fields shown in Figure 2, where a steep increase in velocity in the vicinity of the cathode is due to the Maecker pressure. It is also noted that the higher current (2160 A) of this computation results in a significantly higher maximum velocity (about 4 times larger than in the argon case described previously). The maximum slope and maximum values of velocity and pressure are used to define the characteristic axial length (Z_S) used in the scaling formulation described in the previous section.

Table IV summarizes the characteristic values obtained numerically for a number of arc cases ranging from 200 to 2160 A and including properties of argon and air plasmas.

VI. CORRECTION OF THE ESTIMATION FUNCTIONS

Figure 5 shows a comparison of the estimations of Eqs. [19] through [22] with characteristic values obtained from the numerical analysis described previously. This comparison spans a range of currents of more than one order of magnitude. In all cases, the estimations predict the correct order of magnitude and functional dependence. The difference between the numerical results and the estimations depends mainly on the Reynolds number and the normalized arc length (h/R_C). The other two governing dimensionless

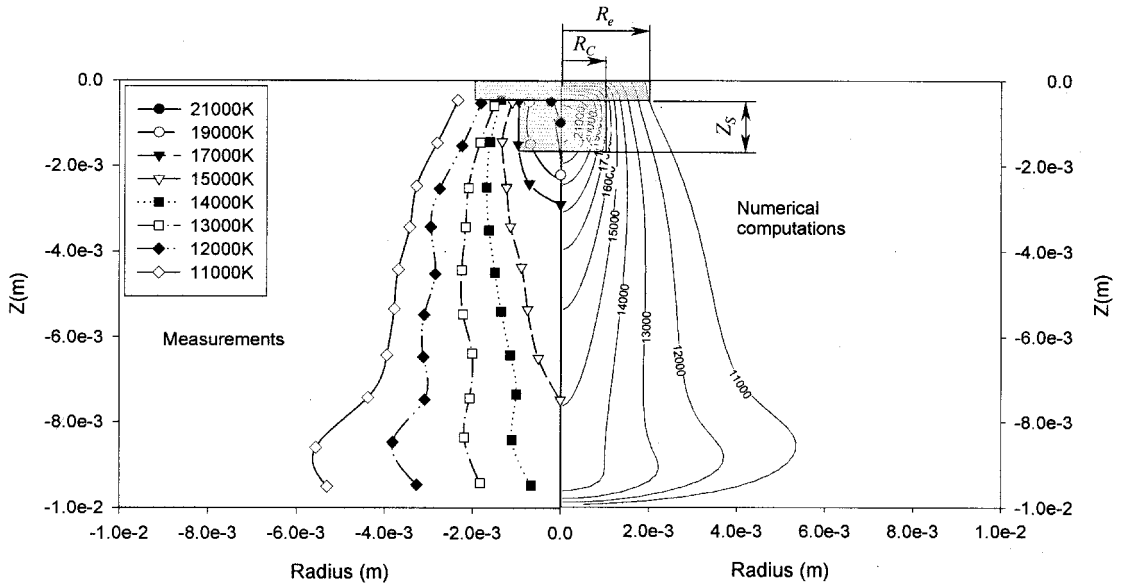

Fig. 3–Comparison between experimental and predicted temperature fields for a 200 A and 10-mm argon arc. The shaded region on top is the boundary layer region, and the shaded region immediately below is the cathode region.

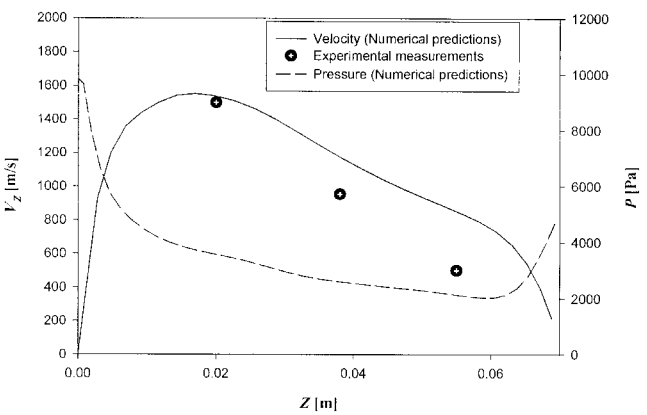

Fig. 4–Calculated axial velocity and pressure profiles along the symmetry axis and velocity measurements from Bowman[25] for a 2160 A and 7 cm air arc.

groups (the dimensionless anode spot R_a/R_C and the dimensionless electrode diameter R_e/R_C) obtained from dimensional analysis are of little influence in this problem. Our analysis of the practical cases studied showed that the Reynolds number and the dimensionless arc length vary considerably (Re ranges from 65 to 2700, and h/R_C ranges from 5 to 36), while the dimensionless anode spot and electrode diameter vary little in comparison (R_a/R_C is approximately 3 and R_e/R_C is approximately 1).

Estimations of the characteristic parameters for fluid flow can be corrected with expressions that depend on the complete set of dimensionless groups. As was explained previously, only two of these groups are significant, and OMS indicates that the corrections should be fairly smooth. Therefore, the characteristic values can be approximated accurately by the following set of equations:

$$Z_S = \hat{Z}_S f_Z\,(\mathrm{Re}, h/R_C) \quad [23]$$

$$V_{RS} = \hat{V}_{RS} f_{VR}\,(\mathrm{Re}, h/R_C) \quad [24]$$

$$V_{ZS} = \hat{V}_{ZS} f_{VZ}\,(\mathrm{Re}, h/R_C) \quad [25]$$

$$P_S = \hat{P}_S f_P\,(\mathrm{Re}, h/R_C) \quad [26]$$

The correction functions of Eqs. [23] through [26] cannot be determined through OMS alone, but, combined with the numerical calculations performed in this work (summarized in Table IV), simplified but accurate expressions in the form of a power law are proposed:

$$f_Z = 0.88\,\mathrm{Re}^{0.058}\,(h/R_C)^{0.34} \quad [27]$$

$$f_{VR} = 0.22\,\mathrm{Re}^{-0.026}\,(h/R_C)^{0.086} \quad [28]$$

$$f_{VZ} = 0.55\,\mathrm{Re}^{0.073}\,(h/R_C)^{0.0068} \quad [29]$$

Table IV. Characteristic Values Obtained through Numerical Analysis

Gas	Electrode	I (A)	h (m)	T_{max} (K)	ρ (kg/m^2)	μ (kg/m s)	R_C (m)	Z_S (m)	V_{RS} (m/s)	V_{ZS} (m/s)	P_S (Pa)
Argon	W	200	0.01	21600	1.12×10^{-2}	5.41×10^{-5}	9.897×10^{-4}	1.22×10^{-3}	76	256	574
Argon	W	200	0.02	21500	1.12×10^{-2}	5.41×10^{-5}	9.897×10^{-4}	1.47×10^{-3}	80	266	597
Argon	W	300	0.0063	23200	9.97×10^{-3}	4.59×10^{-5}	1.212×10^{-3}	1.30×10^{-3}	101	353	1084
Argon	W	300	0.01	23200	9.97×10^{-3}	4.59×10^{-5}	1.212×10^{-3}	1.49×10^{-3}	104	363	1062
Argon	W	300	0.02	23100	9.97×10^{-3}	4.59×10^{-5}	1.212×10^{-3}	1.75×10^{-3}	105	372	989
air	C	520	0.07	17200	5.70×10^{-3}	3.26×10^{-5}	1.940×10^{-3}	4.76×10^{-3}	170	574	1492
air	C	1150	0.07	19500	4.71×10^{-3}	1.87×10^{-5}	2.884×10^{-3}	5.43×10^{-3}	247	983	3653
air	C	2160	0.07	21300	4.23×10^{-3}	1.64×10^{-5}	3.953×10^{-3}	7.09×10^{-3}	318	1498	7524

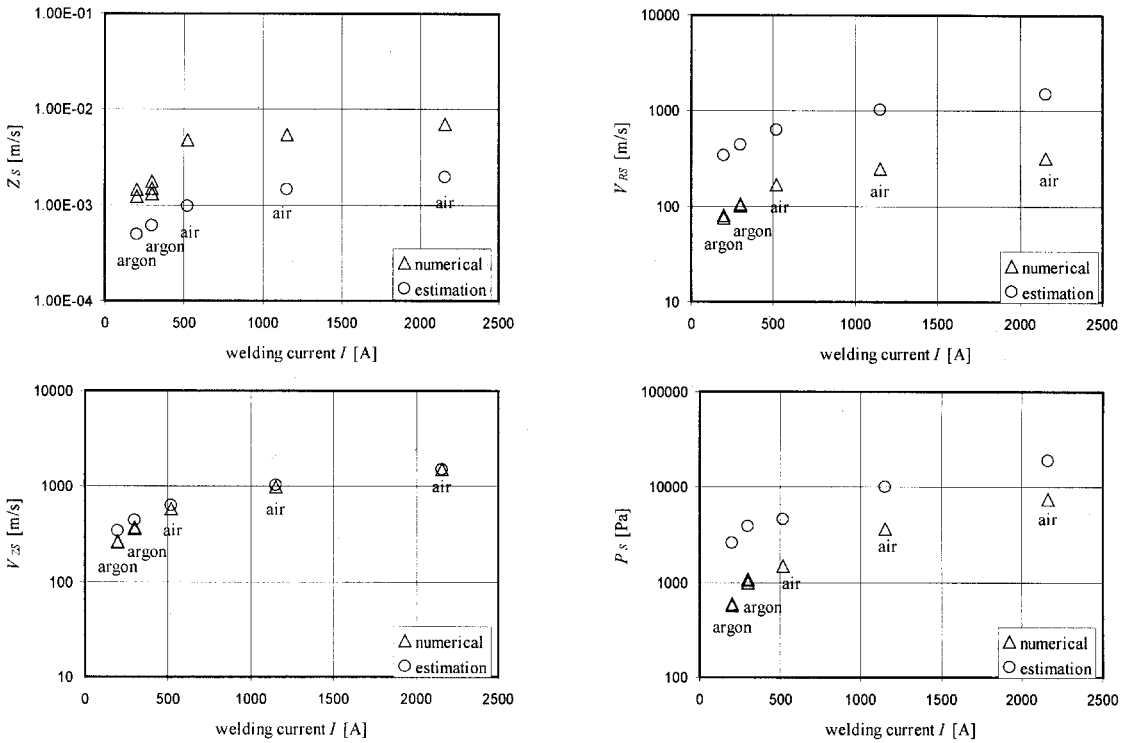

Fig. 5–Estimations and numerical calculations of V_{RS} V_{ZS}, P_S, and Z_S. In all cases, the estimations predict the correct order of magnitude and functional dependence. The difference between numerical results and the estimations depends mainly on two dimensionless groups: Re and h/R_C.

$$f_P = 0.13\ \mathrm{Re}^{0.17}\ (h/R_C)^{-0.057} \qquad [30]$$

The corrected scaling factors can be used to normalize the solutions of the system of equations, such that various different cases converge toward a single dimensionless representation. Figure 6 shows a representation of the normalized radial velocity for the two extreme cases from Table IV: a small 200 A, 10 mm argon arc, and a strong 2160 A, 7 cm air arc. Although the two contour plots do not overlap perfectly in this limiting case, they present similar features, such as the presence and the location of the maximum V_R. The thickness of the cathode boundary layer is unknown. Estimations based on the standard model for a flat plate suggest that the difference in cathode boundary-layer thickness represented in Figure 6 is of the correct order of magnitude.

VII. DISCUSSION

The estimations obtained for maximum velocity and pressure have the same functional form as those previously proposed.[6,8,13] These estimations were extracted from the original set of governing equations by using the OMS technique, which relies on asymptotic considerations and dimensional analysis. This technique does not require the numerical solution of the original system of differential equations, neither to impose functional forms of the solutions nor to assume *a priori* which the dominant forces are. The goal of the estimations obtained here is to provide the correct functional dependence and the proper order of magnitude of the solutions. Equation [22], which provides an estimate of a characteristic pressure in the cathode region, is exactly the same as that obtained by Maecker. Equation [21], which provides an estimate of a characteristic axial velocity, is a better approximation than Maecker's equivalent expression (Maecker's numerical coefficient overestimates the maximum velocity, while the coefficient obtained here generates estimations closer to the actual values). The previously existing approximate algebraic expressions can be improved with the use of a constant correction factor, as done by McKelliget and Szekely.[20] The drawback of that approach is that a constant fitting factor cannot include the phenomena that were neglected in obtaining the simplified algebraic expression. The functions of Eqs. [27] through [30] proposed here fulfill the role of a correction factor, but their functional dependence is clearly understood. The small exponents in the power-law expressions indicate that the estimations capture the essence of the behavior of the solution. The exponent of h/R_C in f_Z is significantly larger than all the other exponents, suggesting that Z_S is particularly sensitive to the arc length.

The hypothesis of laminar flow in the cathode region is justified by analyzing the onset of turbulence in an axisymmetric jet, which corresponds to a Reynolds number (based on measured velocity, not estimated) of the order of 10^5.[20] All of the cases analyzed here have true Reynolds numbers smaller than 3×10^3. If fluid flow depended only on Re and h/R_C (as is assumed in Eqs. [27] through [30]), the exact solution could be expressed by Eqs. [23] through [26]; however, the actual problem depends on many more parameters, some of which include thermal properties and variations in these properties. The effect of the simplifications made to the scaling of this problem is translated into an error around the corrected values, with the magnitude of this error indicative of the quality of the simplifications. For the cases

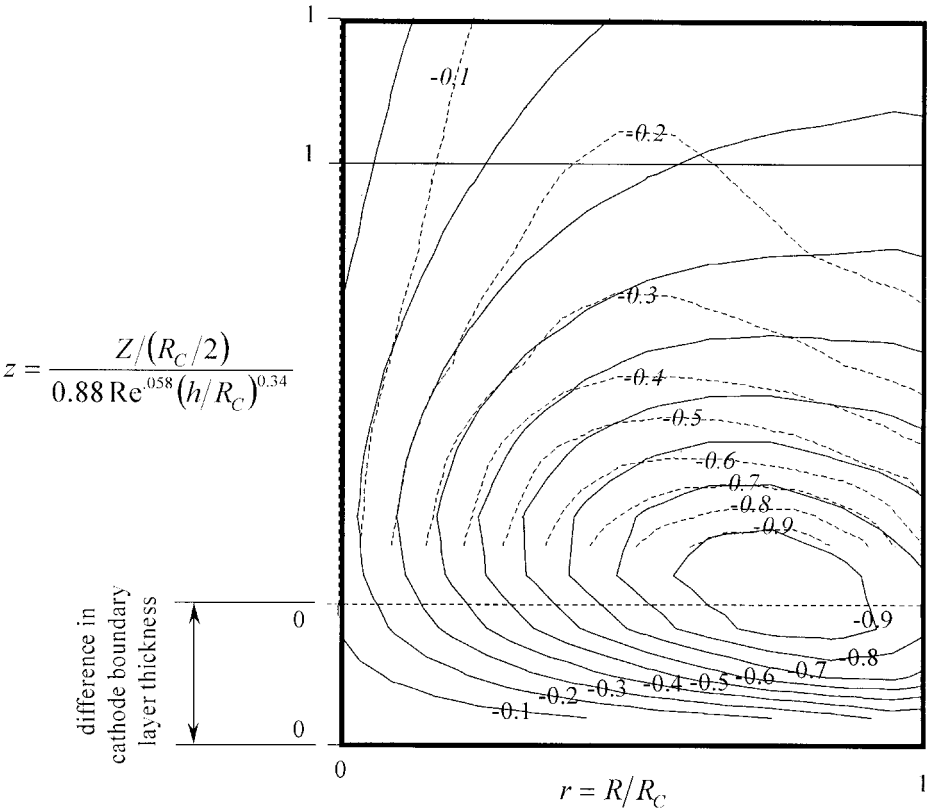

Fig. 6–Normalized contour plot of VR(R, Z)/VRS for the numerical calculations of an argon arc of 200 A and 10-mm length (solid lines) and for an air arc of 2160 A and 7-cm length (dashed lines, italicized numbers). These two very different arcs converge to similar normalized representation by using OMS and considering the effect of the cathode boundary layer.

shown in Table IV, the maximum error for f_Z is 13 pct, that for f_{VR} is 6 pct, that for f_{VZ} is 3 pct, and that for f_P is 8 pct. The small magnitude of these errors suggests that mainly the Reynolds number and the dimensionless arc length govern the cathode region of an arc.

The advantage of OMS is illustrated in Figure 6. This involves the potential capability of representing universal maps of the important process variables such as velocity components, pressure fields, and the like. For example, the figure shows the normalized radial velocity field, which was obtained using dimensionless groups derived using this technique. As seen in the figure, the contour maps for two extreme conditions (welding arcs of 200 A in argon and 2160 A in air) are plotted, and good agreement is obtained. It is envisioned that by extending the region of analysis and including thermal effects, universal representations can be obtained for the entire arc.

VIII. CONCLUSIONS

The focus of this article involved the application of an OMS technique to represent the behavior of an electric arc. The analysis is centered only in the cathode region, where momentum and electromagnetic phenomena are dominant and temperature effects can be appropriately disregarded (by assuming a region of constant temperature). This technique has been coupled with results obtained from a mathematical model that covered two different gases and a wide range of currents and arc lengths.

The main conclusions of this work can be summarized as follows

1. In the cathode region, the viscous effects are small, and the radial and axial inertial forces balance the electromagnetic pressure created by the flow of the current through the plasma.
2. Estimations of the characteristic values of maximum velocity and maximum pressure obtained through OMS have the same functional dependence as previous analytical expressions determined by Maecker[8] and Allum.[13]
3. The maximum velocity and pressure estimations are given by the following equations, derived using OMS:

$$\hat{V}_{RS} = \frac{1}{2}\frac{\mu_0^{1/2} R_C J_C}{\rho^{1/2}}$$

$$\hat{V}_{ZS} = \frac{1}{2}\frac{\mu_0^{1/2} R_C J_C}{\rho^{1/2}}$$

$$\hat{P}_S = \frac{1}{2}\mu_0 R_C^2 J_C^2$$

4. When compared with numerical results, the previous estimation of maximum axial velocity provides a better prediction than Maecker's corresponding expression (these expressions differ by a factor of $\sqrt{2}$). The expression for estimated maximum pressure is exactly the same as that previously obtained by Allum and Maecker.
5. The velocity and pressure estimations can be refined with independent information obtained from numerical

Table V. Summary of Magnitudes, Associated Functions, Characteristic Values, and Estimations Used in the Formulation of the Problem

Magnitude	Symbol	Normalized Magnitude	Characteristic Value	Estimated Characteristic Value	Correction Function
Radial coordinate	R	r	R_C	–	–
Axial coordinate	Z	z	Z_S	$\hat{Z}_S$	$f_Z(\mathrm{Re}, h/R_C)$
Radial velocity	$V_R(R, Z)$	$v_r(r, z)$	V_{RS}	$\hat{V}_{RS}$	$f_{VR}(\mathrm{Re}, h/R_C)$
Axial velocity	$V_Z(R, Z)$	$v_z(r, z)$			$f_{VZ2}(\mathrm{Re}, h/R_C)$
		$v_{z0}(z)$	V_{ZS}	$\hat{V}_{ZS}$	$f_{VZ}(\mathrm{Re}, h/R_C)$
Pressure	$P(R, Z)$	$p(r, z)$	P_S	$\hat{P}_S$	$f_P(\mathrm{Re}, h/R_C)$
Radial current density	$J_R(R, Z)$	$j_r(r, z)$	J_{RS}	$\hat{J}_{RS}$	–
Axial current density	$J_Z(R, Z)$	$j_z(r, z)$	J_C	–	–
Magnetic flux density	$B(R, Z)$	$b(r, z)$	B_S	–	–

or experimental results. These refinements depend on the Reynolds number and the normalized arc length. Because these correction factors depend on the most relevant dimensionless groups in the cathode region, they present a further refinement of corrections based on constant factors, such as the correction of Maecker's formula proposed by McKelliget and Szekely.[20]

6. Potentially, the refined estimations can be used to normalize the fields given by numerical results in such a way that these fields converge into universal maps of important process variables.

NOTATION

A summary of the magnitudes, associated functions, characteristic values, and estimations used in the formulation of the problem is presented in Table V. The other symbols used in this work are as follows.

h	arc length
J_c	current density at cathode
k	number of dimensionally independent parameters (elements of set $\{P_k\}$)
m	number of independent dimensionless groups (elements of $\{\Pi\}$)
n	number of parameters in a problem (elements of $\{P\}$)
$\{P\}$	set of parameters
$\{P_k\}$	subset of $\{P\}$ of dimensionally independent parameters
R_a	anode spot radius
R_c	cathode spot radius
R_e	radius of electrode
Re	Reynolds number
Re_m	magnetic Reynolds number
δ	cathode boundary-layer thickness
ΔR	variation of radius between the cathode and anode
μ	viscosity of the plasma at the maximum temperature in the arc
μ_0	permitivity of free space
$\{\Pi\}$	complete set of dimensionless groups
ρ	density of the plasma at the maximum temperature in the arc
σ_e	electric conductivity of the plasma at the maximum temperature in the arc

REFERENCES

1. P.F. Mendez: Ph.D. Thesis, Massachusetts Institute of Technology, Cambridge, MA, 1999.
2. C.M. Bender and S.A. Orszag: *Advanced Mathematical Methods for Scientists and Engineers*, 1st ed., McGraw-Hill, New York, NY, 1978.
3. M.M. Chen: *Annual Review of Heat Transfer*, 1st ed., Hemisphere Pub. Corp., New York, NY, 1990, pp. 233-91.
4. G. Astarita: *Chem. Eng. Sci.*, 1997, vol. 52, pp. 4681-98.
5. G.I. Barenblatt: *Scaling, Self-Similarity, and Intermediate Asymptotics*, 1st ed., Cambridge University Press, New York, NY, 1996.
6. J.W. McKelliget and J. Szekely: *J. Phys. D: Appl. Phys.*, 1983, vol. 16, pp. 1007-22.
7. H.B. Squire: *Q. J. Mech. Appl. Math.*, 1951, vol. IV, pp. 321-29.
8. H. Maecker: *Z. Phys.*, 1955, vol. 141, pp. 198-216.
9. O.I. Yas'ko: *B. J. Appl. Phys. (J. Phys. D)*, 1969, vol. 2, pp. 733-51.
10. J.A. Shercliff: *J. Fluid Mech.*, 1970, vol. 40, pp. 241-50.
11. D.C. Strachan and M.R. Barrault: *J. Phys. D: Appl. Phys.*, 1976, vol. 9, pp. 435-46.
12. T.D. Burleigh: Master's Thesis, Massachusetts Institute of Technology, Cambridge, MA, 1980.
13. C.J. Allum: *J. Phys. D: Appl. Phys.*, 1981, vol. 14, pp. 1041-59.
14. B. Bowman: *Properties of Arcs in DC Furnaces*, 52nd Electric Furnace Conference, Nashville, TN, 13-16 Nov., 1994, pp. 111-20.
15. K.C. Hsu, K. Etemadi, and E. Pfender: *J. Appl. Phys.*, 1983, vol. 54, pp. 1293-1301.
16. J. McKelliget and J. Szekely: *The Modelling of Fluid Flow and Heat Transfer in Arc Furnaces*, 5th Arc Furnace Meeting, Budapest, Hungary. 24-27 September, 1985, 1985.
17. M. Goodarzi, R. Choo, and J.M. Toguri: *J. Phys. D: Appl. Phys.*, 1997, pp. 2744-56.
18. J.J. Lowke, R. Morrow, and J. Haidar: *J. Phys. D: Appl. Phys.*, 1997, vol. 30, pp. 2033-42.
19. W.-H. Kim, H.G. Fan, and S.-J. Na: *Metall. Mater. Trans. B*, 1997, vol. 28B, pp. 679-86.
20. J. McKelliget and J. Szekely: *Metall. Trans. A*, 1986, vol. 17A, pp. 1139-48.
21. G.R. Jordan, B. Bowman, and D. Wakelam: *J. Phys. D: Appl. Phys.*, 1970, vol. 3, pp. 1089-99.
22. C. Moffat: *Developments in Heat Transfer*, 1st ed., MIT Press, Cambridge, MA, 1964, pp. 107-33.
23. E. Buckingham: *Phys. Rev.*, 1914, vol. 4, pp. 345-76.
24. R. Morrow and J.J. Lowke: *J. Phys. D: Appl. Phys.*, 1993, vol. 26, pp. 634-42.
25. B. Bowman: *J. Appl. Phys.*, 1972, vol. 5, pp. 1422-32.